Interpretation of gravity wave signatures in GPS radio occultations

P. Alexander,[1] A. de la Torre,[1] and P. Llamedo[1]

[1] The horizontal averaging of global positioning system radio occultation retrievals produces an amplitude attenuation and phase shift in any plane gravity wave, which may lead to significant discrepancies with respect to the original values. In addition, wavelengths cannot be straightforwardly inferred due to the observational characteristics. If the waves produce small departures from spherical symmetry in the background atmosphere and under the assumption that the refractivity kernel may be represented by a delta function, an analytical expression may be derived in order to find how the retrieved amplitudes become weakened (against the original ones). In particular, we study the range of waves that may be detected and the consequent reduction in variance calculation, which is found to be around 19%. A larger discrepancy was obtained when comparing an occultation variance with the one computed from a numerical simulation of that case. Wave amplitudes can be better resolved when the fronts are nearly horizontal or when the angle between the occultation line of sight and the horizontal component of the wave vector approaches $\pi/2$. Short horizontal scale waves have a high probability of becoming attenuated or of not being detected at all. We then find geometrical relations in terms of the relative orientation between waves and sounding, so as to appropriately interpret wavelengths extracted from the acquired data. Only inertio-gravity waves, which exhibit nearly horizontal fronts, will show small differences between detected and original vertical wavelengths. Last, we analyze the retrieval effect on wave phase and find a shift between original and detected wave that generally is nonzero and approaches $\pi/4$ for the largest horizontal wavelengths.

1. Introduction

[2] Different sounding techniques have been employed in the last decades to explore lower- and middle-atmosphere physics and chemistry. Data have been acquired by means of in situ (measurement devices on board of rockets, balloons and aircraft) as well as remote ground- (radars and lidars) and space-based methods (sensors in satellites). A suite has particularly emerged in the latter group in the last decade using limb or nadir paths to obtain refractivity, density, temperature, pressure and water vapor content in the neutral atmosphere. Among various topics, these observations have been used to study gravity waves (GW) mainly in the stratosphere [e.g., *Wu and Waters*, 1996; *Tsuda et al.*, 2000; *Preusse et al.*, 2002; *de la Torre and Alexander*, 2005]. In the present study we focus on one of the limb techniques presently providing a huge amount of atmospheric information, the so-called Global Positioning System (GPS) radio occultation (RO). The aim of this method is to detect the perturbation in Doppler frequency produced by refractive bending of the signal in a limb path between a transmitter and a receiver in the occultation plane defined also by the Earth center (Figure 1). The horizontal refractivity variations normal to this plane have a negligible bending effect [*Lusignan et al.*, 1969]; therefore, the amount of refraction experienced by the ray depends on the refractivity distribution in the plane of occultation. In the absence of water vapor, the refractivity varies linearly with density. If spherical symmetry is assumed, then the set of values provided by the whole occultation leads to a slant profile of atmospheric parameters against successive tangent point positions. The resolution is quite good (up to a few hundred meters) and much lower (up to a few hundred kilometers) in the vertical and horizontal directions, respectively [e.g., *Wu et al.*, 2006]. The advantages as compared to other options are that this technique is nearly an instantaneous snapshot (typically 1 min as compared to the much longer atmospheric processes), it has a global coverage, sub-Kelvin accuracy in temperature measurements from the upper troposphere to the lower stratosphere, and it is not interrupted by clouds or weather conditions.

[3] GW amplitudes and potential energies obtained from GPS RO have been generally found to be smaller than those obtained by other methods and phase shifts between the corresponding temperature profiles have also been found [see, e.g., *Ratnam et al.*, 2004]. Although some evaluations of the GPS RO method's limits and ranges of applications

[1]Departamento de Física, Facultad de Ciencias Exactas y Naturales, Universidad de Buenos Aires, Buenos Aires, Argentina.
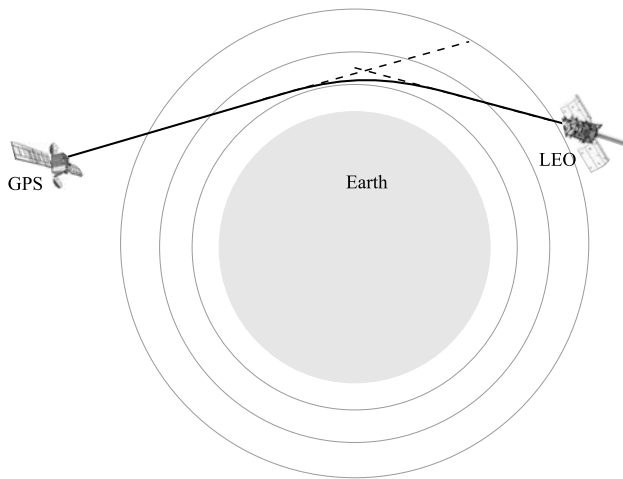
Figure 1. Refractive bending in the Earth atmosphere of a signal between transmitter and receiver satellites in a GPS RO. The deviation angle has been exaggerated for illustration purposes.

on inhomogeneities [*Gorbunov*, 1990] or GW have been presented [e.g., *Belloul and Hauchecorne*, 1997; *Lange and Jacobi*, 2003; *Wu et al.*, 2006], some aspects have not been assessed or remain unclear. For example, the effects produced by the particular oblique geometry of the technique in reference to wavelength detection have seldom been mentioned. Because of the departure from horizontal or vertical sounding lines, the detected wavelengths must be distinguished from the original horizontal or vertical ones, and appropriately interpreted in relation to wave vector and sounding directions. Moreover, as limb sounding paths are directed far away from the vertical, the nonhorizontality of phase surfaces introduces a systematic discrepancy between original and apparent (detected) vertical wavelengths (most studies focus on quantities associated to the observed vertical wavelength). This difference will be more or less significant, depending on the phase surface inclination of the wave structures observed (see an analogy for measurements from balloons in *de la Torre and Alexander* [1995]). The difference is expected to be greater for mountain waves (MW) than for inertia-gravity waves (IGW), as the phase surfaces of the latter are nearly horizontal. It is even possible that some waves will not be resolved or that they will be found shifted due to the smearing along the raypath. In *de la Torre and Alexander* [2005] it was emphasized that the capability of limb-sounding devices and, in particular, GPS RO experiments on board of low Earth orbit satellites, to detect typical mountain waves with horizontal wavelengths shorter than 150 km, depended on the horizontal angle between the line of sight (LOS) and the wave phase surfaces to be detected. As GPS RO observations also provide a widely used tool to estimate temperature variance and potential energy, this may in turn affect global gravity wave activity calculations. In brief, it becomes necessary to delimit which waves may be detected and then to quantify how their extracted parameters will be affected by the characteristics of the method.

[4] In order to find out the lower bounds for detectable GW signatures and to be able to interpret these patterns in

real data, it is necessary to have a knowledge on the general GPS RO retrieval response to different wave parameters and to know the relative orientation between wave and sounding in each case. In the following section we derive analytical expressions in order to relate original and measured amplitudes, wavelengths and phases and, in particular, we study the range of plane waves that may be detected. Most data sets obtained from radio occultation measurements are based on the Abel transform linking refractivity gradient and ray bending [see, e.g., *Fjeldbo et al.*, 1971] under the consideration of spherical symmetry. The assumptions of a dry atmosphere, an exponential decrease of atmospheric density with altitude, a linear relationship between refractivity and density, hydrostatic equilibrium and the perfect gas law and again spherical symmetry lead to profiles of pressure, temperature and density. In addition, a uniform and constant basic horizontal wind speed is implicitly considered to infer waves (to ensure a nonvarying vertical wavelength, see *Alexander* [1998]). Atmospheric deviations from all these hypotheses lead to uncertainties in the retrieved profiles. It becomes difficult to assess the effects of departure from spherical symmetry because, among other things, one cannot isolate the consequences on the transform of particular points along the ray. We therefore use an equation relating the one-dimensional (1D) retrieved and two-dimensional (2D) original refractivities through a profile retrieval 2D mapping kernel [*Ahmad and Tyler*, 1998], and study the ability to detect the effects by GW assuming that they induce small departures from sphericity in the background atmosphere. These considerations keep the problem of amplitude and phase analytically tractable. We also find geometrical relations so as to appropriately interpret horizontal and vertical wavelengths extracted from the acquired data.

2. Interpretation of GW Parameters Extracted From GPS RO Retrievals

[5] We first study the relation between original and observed wave amplitudes in GPS RO retrievals, in particular if any ranges or thresholds of detectable oscillations may be determined. Then we analyze how the wavelengths and phases become affected.

[6] Before we proceed with the analytical treatment, we perform some intuitive qualitative assessments of the expected differences between every detected wave and the corresponding original signal due to the smearing effect of occultations and the relative orientation of wave and observation. We consider three simple cases and then extend them without any formality to the most general situation. In Figure 2a the LOS corresponding to a given tangent point of an occultation is parallel to the horizontal component of the wave vector (as is known, the LOS is contained in the horizontal plane around the tangent point). In this case, only a weak signature, if any, will be detected because the integrated measure along the LOS will tend to be canceled out by successive positive and negative contributions of the wave. If a signal is indeed detected, then the apparent horizontal and vertical wavelengths will differ from the original ones because the successive tangent points are neither on a horizontal nor on a vertical straight line, but rather on a slant line (this is a characteristic of limb
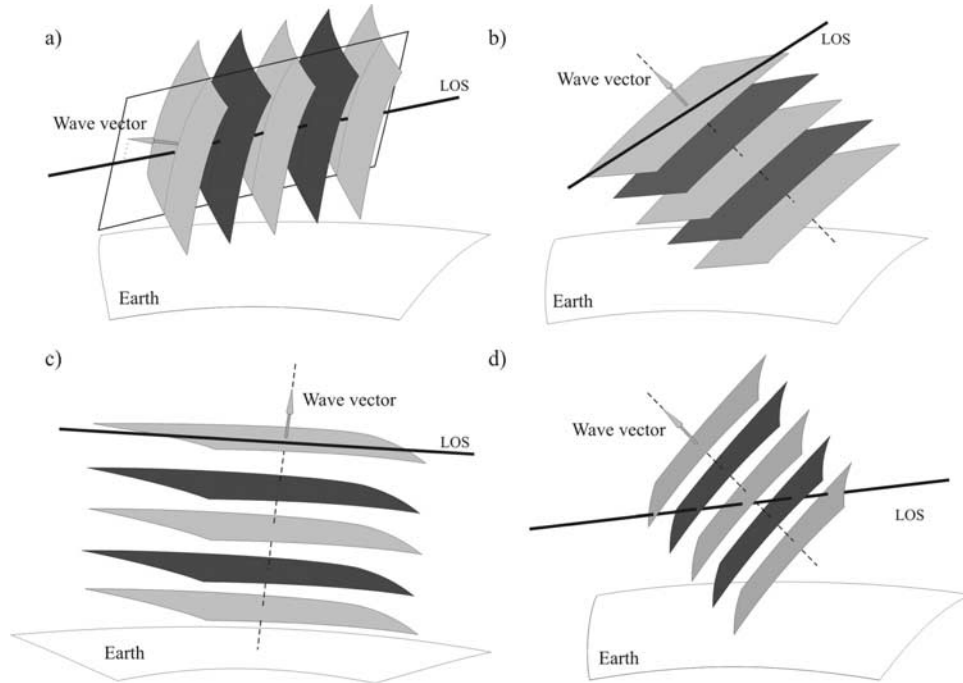
Figure 2. Representation of the relative orientation of wave and LOS in three simple cases (a) horizontal component of wave vector parallel to LOS, (b) LOS contained in wavefront and (c) horizontal wavefronts, whereas Figure 2d shows the most general situation.

techniques like GPS RO). If all the tangent points are located by chance on the same wavefront, then no amplitude changes will be detected and the wavelengths will be apparently infinite. Figure 2b shows a LOS contained in a wavefront, so the smearing along the LOS is performed on a constant phase surface and therefore no successive cancellations will occur. This optimal situation for wave amplitude detection will break down only if the successive tangent points fall by chance on the same wavefront. The same arguments on wavelengths as above apply to this case. In Figure 2c we see horizontal wavefronts (typically IGW). As the LOS is also horizontal, this represents again an optimal situation for amplitude observation (integrated measure over a constant phase surface). A faithful vertical wavelength will be revealed by the measurement at successive tangent points but a wrong apparent horizontal wavelength will be found (the true one is infinite). Figure 2d represents the most general case, where an amplitude between null and the original one will be measured and where the horizontal and vertical wavelengths will become distorted by the relative orientation of the observation and the wave. The phase shift is related to the fact that the retrieved values correspond to weighted integrals along the raypath crossing the wave rather than to point measurements.

[7] Although the explanations below may lead to an understanding of the effect on each mode, the outcome of an occultation in the real atmosphere is the aggregate of a very complex three-dimensional (3D) combination of waves and other local and global phenomena. In single occultation events, unless there is a single, clean dominant mode where the parameters do not significantly vary with height, the practical application of this study relies on collective

characteristics like variance. Some of the results below may be applied to climatologies by statistical means.

2.1. Amplitude Attenuation

[8] We now resort to the 2D mapping kernel for the retrieval of refractivity profiles by Abelian transformation of radio occultation data given by equation (10) by *Ahmad and Tyler* [1998]

$$\tilde{\nu}(\varrho) = 2 \int_0^\infty \int_{-\infty}^\infty dX \, dZ \, \kappa(Z; \varrho)\nu(X, Z) \tag{1}$$

where $\nu(X, Z)$ and $\hat{\nu}(\varrho)$ respectively are the original and retrieved refractivities, X, Z and ϱ respectively represent the horizontal and vertical directions and the radial coordinate of the tangent point in the occultation plane (see Figure 3) and κ is the system impulse response. This κ function is not well behaved as it has a doubly infinite discontinuity in the neighborhood of the tangent point. In general, the problem is overcome by using a wave number domain windowed alternative, which is in agreement with standard data processing. However, we wish to keep the solutions below independent from any particular filtering process. As spherical symmetry corresponds to a δ function like resolving kernel [*Ahmad and Tyler*, 1998], we will assume that the small perturbations induced by the GW in the spherically symmetric background atmosphere allow the kernel to be closely represented by a δ function in the direction perpendicular to the ray in the occultation plane around the tangent point. This shows some similarities with the 2D solution by *Ahmad and Tyler* [1998], although their function goes from 0 below to
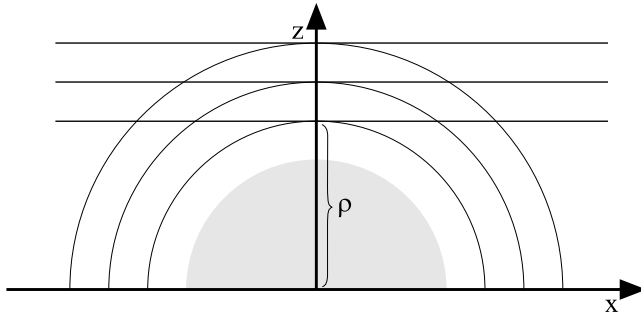
Figure 3. Cartesian coordinates (X, Z), radial coordinate of the tangent point ρ and successive raypaths (small curvature compared to the Earth surface) shown as parallel lines connecting receiver and transmitter satellites in the occultation plane.

infinite at the ray position and jumps to $-\infty$ immediately above and remains negative thereafter, whereas the integral over space remains ambiguous. Similarly to other perturbative schemes, this approach may remain valid as long as the departure from spherical symmetry brought to the background by the GW is small, i.e., the refractivity perturbation must not exceed a first order modification of the basic state, because otherwise the kernel will significantly depart from a δ. The kernel simplification keeps the problem analytically tractable, avoiding complications that would obscure or even impede the necessary interpretation of GW GPS RO observations. This approach to the problem may limit the accuracy of the results given below, but they still may be representative of the analyzed system and reveal its basic aspects.

[9] Apart from the small deviations from spherical symmetry due to the GW, the development of our work includes the following usual additional assumptions or simplifications: the bending of the ray is negligible as compared to the Earth's curvature, the region crossed by the signal is optically thin and the background atmosphere is isothermal with scale height $H = 7.3$ km (the temperature variability in the troposphere and lower stratosphere may lead to local departures from this value up to 15%). The refractivity field $\nu(X, Z)$ will be represented by a background spherically symmetric exponential radial component and a first order field induced by a GW:

$$
\begin{aligned}
\nu(x,z) &= \nu_o(z) + \nu_1(x,z) \\
&= \nu_B \exp(-z/H)(1 + A\sin(kx + mz + \phi)) \quad (2)
\end{aligned}
$$

where k and m respectively are the horizontal and vertical wavelengths, A is a first order nondimensional amplitude and ν_B represents the background refractivity at a reference level. As is known, refractivity is proportional to density, and density and temperature fluctuations are basically in phase opposition in a GW [*Eckermann et al.*, 1998]. In Figure 4, note that in the occultation plane X and Z represent the coordinates of a point in a Cartesian system, whereas x and z correspond to a polar-like reference frame ($x = 0$ is the line connecting the Earth center and a given tangent point, $z = 0$ is the circle around the Earth center passing through the tangent point). As the integral of

equation (1) will be performed along the ray, we need to link X with the horizontal and vertical separations x and z. It is easy to see that, for a small azimuthal angle (less than $2°$ from the vertical direction in the region where the exponential weighting exceeds half its peak value)

$$
z \approx \frac{X^2}{2R_E} \quad \text{and} \quad x \approx X \quad (3)
$$

where $R_E = 6400$ km is the Earth radius.

[10] The first order contribution of the small disturbance induced by the GW is

$$
\hat{\nu}_1(\varrho) = \int_{-\infty}^{\infty} \nu_B \exp(-X^2/(2R_E H)) A \sin(kX + mX^2/(2R_E) + \phi) dX \quad (4)
$$

After using an angle addition identity for the sine function and removing the odd parts it is possible to find an analytical solution [*Gradshteyn and Ryzhik*, 1965] to the integral (*Belloul and Hauchecorne* [1997] did not realize that they could have skipped their numerical solutions for the bending angle with the corresponding integral solution). In addition, some algebra after noting that $Hm \gg 1$ may be assumed (roughly vertical wavelength $\lambda_z = 2\pi/m \leq 10$ km) gives

$$
\hat{\nu}_1(\varrho) = \nu_B A \exp\left(-\frac{1}{2}\frac{k^2}{m^2}\frac{R_E}{H}\right)\sqrt{\frac{2\pi R_E}{m}}\sin\left(\phi - \frac{k^2 R_E}{2m} + \pi/4\right) \quad (5)
$$

Note that the GPS RO method can appropriately infer waves when the detected λ_z, which will usually differ from the original value, is not larger than 10 km [see, e.g., *Wu et al.*, 2006]. The zero order refractivity due to the background atmosphere along the raypath is

$$
\hat{\nu}_0(\varrho) = \int_{-\infty}^{\infty} \nu_B \exp(-X^2/(2R_E H)) dX = \nu_B \sqrt{2\pi H R_E} \quad (6)
$$

Some appropriate calibration factor should be included in equations (4), (5) and (6) in order to deal with the refractivity,
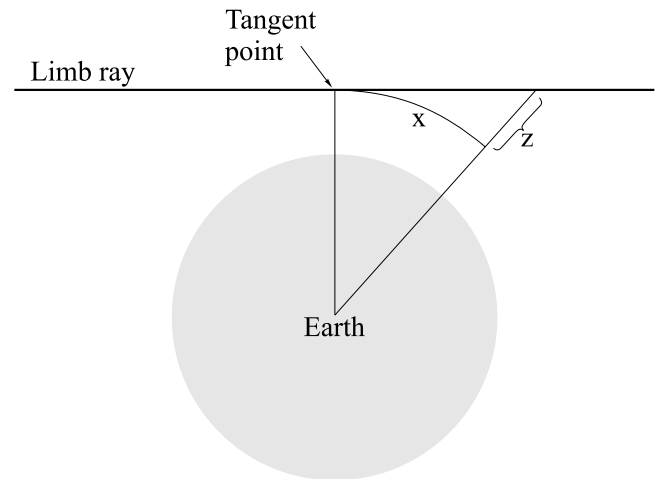

Figure 4. Polar-like reference frame (x, z) with the origin at the tangent point. This coordinate system is used to calculate the integrated measure of refractivity along the raypath.
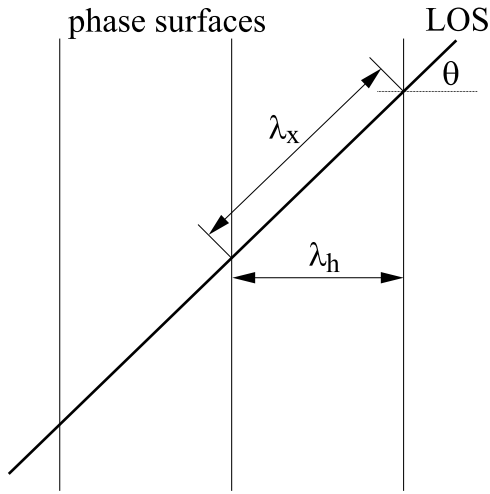
Figure 5. LOS angle θ with respect to the horizontal projection of the wave vector and the "true horizontal" and "along LOS" wavelengths λ_h and λ_x. A simplified 2D geometry leads to $\theta = 0$ and $\lambda_x = \lambda_h$.

including its right unit, because the expressions represent an integrated measure of that quantity in the path traversed by the ray. For the perturbation to background refractivity ratio (or apparent relative amplitude), which we call the response, we obtain:

$$R = A \, \exp\left(-\frac{1}{2}\frac{k^2}{m^2}\frac{R_E}{H}\right)\sqrt{\frac{1}{Hm}}\sin\left(\phi - \frac{k^2 R_E}{2m} + \pi/4\right)$$
$$= A(k,m)E(k,m)D(m)S(k,m) \tag{7}$$

We point out that $k = 0$ corresponds to spherical symmetry, which exhibits no exponential attenuation. As *Belloul and Hauchecorne* [1997] have already shown, small k waves do slightly depart from spherical symmetry due to their geometry. They have also stated that large k waves become attenuated with respect to the original signal, which leads to a closer match to spherical symmetry. Finally, they showed that the intermediate range introduces the largest retrieval errors due to the spherical symmetry breakdown.

[11] The term $D = 1/\sqrt{Hm}$ tends to attenuate the response to short vertical wavelengths. We follow the arguments by *Preusse et al.* [2002] for an infrared limb sounder in assuming that this vertical degradation may be overcome with an infinite signal-to-noise ratio of an ideal instrument. We therefore define

$$R' = \frac{R}{(ED)_{k=0}} = \frac{R}{D} \tag{8}$$

which implies the removal of the background degradation in absence of horizontal variations. As $S = \sin(\phi - \frac{k^2 R_E}{2m} + \pi/4)$ reflects the phase shift between the original and the detected wave (see below), we ignore it for the moment and consider

$$R'' = \frac{R'}{S} = \frac{R}{DS} \tag{9}$$

The retrieved refractivity accuracy for the upper troposphere and lower stratosphere has been estimated in successive studies [*Rieder and Kirchengast*, 2001; *Yunck*, 2002; *Kuo*

et al., 2004] and the latest results reveal values lower than 0.2% [*Schreiner et al.*, 2007]. A necessary condition in wave number space for the detection of waves follows from $R'' > 0.002$: $A(k, m) > 0.002/E(k, m)$. For a typical GW, $A \sim 0.005 - 0.03$ and we will consider a uniform $A = 0.02$. Then, the perturbations may be detected if (E may now be interpreted as the ratio between derived and original amplitudes, a kind of retrieval attenuation factor) $R''/A = E > 0.1$. Note that this condition is a function solely of the vertical to horizontal scales (given by the wavelengths) aspect ratio

$$\alpha = \frac{k}{m} \equiv \frac{\lambda_z}{\lambda_x} \tag{10}$$

and implies that the inclination angle of the wavefronts with respect to the horizontal plane must be smaller than 4.1° or larger than 175.9° (if the angle is defined between 0 and 180°). If we assume a uniform distribution of the wave spectrum in the range 2 km $\leq \lambda_z \leq$ 10 km and 25 km $\leq \lambda_x \leq$ 1000 km, then E yields that 63% of the waves are retrieved with an amplitude higher than 0.9 times the original one and the variance is 0.73 times the original one. As shown below, this 2D geometry represents the worst case and therefore implies a lower bound.

[12] The no attenuation situation $k = 0$ emerges from the fact that the ray is then coaligned with the GW constant phase surface (it is a line rather than a plane as, for the moment, we are considering a 2D model), particularly around the tangent point, which is the dominant region for the integral in equation (4). Considering successive tangent points, different constant phase surfaces will be clearly highlighted and the vertical wavelength will be observed. On the contrary, a horizontal angle between LOS and wavefronts significantly different from 0 or π leads to a nearly full smearing out of the wave along the ray, which apparently implies that only a small range of IGW could be detected by the GPS RO method. However, the above calculations are based on a 2D geometry, but the true configuration is 3D. Up to now it has been implicitly assumed that the LOS coincides with the horizontal projection of the wave vector, but this may occur just by chance. In fact, this is a worst case already presented above (see Figure 2a), which will occur rarely. We may extend our 2D results keeping in mind that the above horizontal wavelengths should be called "along LOS". Figure 5 shows how the LOS angle θ with respect to the horizontal projection of the wave vector relates "true horizontal" and "along LOS" horizontal wavelengths (λ_h and λ_x). As the LOS is contained in the horizontal plane around the tangent point, we may assume that in the region with the largest contribution to the integral in equation (4)

$$\lambda_h = \lambda_x \cos\theta \tag{11}$$

This relation may then be inserted into $R'' > 0.002$, leading to a much larger spectrum of waves that exceed a given threshold, i.e., that may be discriminated against the signal of the background, given by the aspect ratio condition

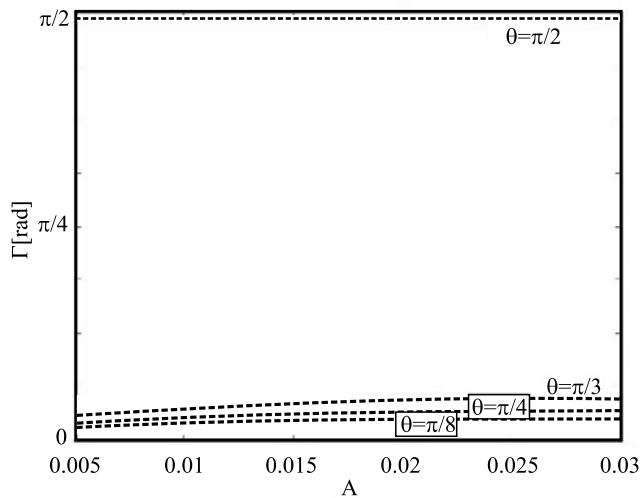$$\alpha_h = \frac{k_h}{m} < \frac{\sqrt{\frac{2H}{R_E}\ln\left(\frac{A}{0.002}\right)}}{\cos\theta} \tag{12}$$

Figure 6. Upper limit inclination angle Γ of the wavefronts with respect to the horizontal surface that leads to over-coming of the measurement threshold due to the occultation smearing. It is represented in terms of the nondimensional wave amplitude A and the angle θ between the LOS and the horizontal projection of the wave vector.

As one may not know the geometry of the original field (i.e., θ), an evaluation of the potential detection of those waves may be only performed in regions where there is a generally preferred orientation of the wavefronts. The tilt angle of the wavefronts with respect to the horizontal surface is γ ($\alpha_h = |\tan(\gamma)|$, $0 \leq \gamma \leq \pi$). In Figure 6, we represent in terms of A and θ the upper limit Γ of γ (due to symmetry we plot for $0 \leq \gamma \leq$

$\pi/2$) that leads to an overcoming of the measurement threshold

$$\gamma < \Gamma = \arctan\left(\frac{\sqrt{\frac{2H}{R_E}\ln\left(\frac{A}{0.002}\right)}}{\cos\theta}\right) \quad (13)$$

If θ is 0 the LOS and horizontal wave vector directions coincide and from equation (13) only waves with a tilt smaller than 4.1° may be detected. Note that $\theta = 0$ is a worst case as discussed above. For rising θ the maximum observable tilt increases and the detectable wave range expands. When $\theta = \pi/2$ is approached, even the most vertical wavefronts can be observed. It must be pointed out that $\theta = \pi/2$ is an ideal observational condition because the smearing along the LOS occurs along the horizontal direction where the wavelength of the plane wave approaches infinite, so the measurement becomes quite representative of a constant phase surface. Note that the detectable range depends mainly on θ, the dependence on A is not so strong. The angle θ may have a random nature between $-\pi/2$ and $\pi/2$. Taking this into account we find that, in average, for a large number of occultations in the 3D case, waves with $\gamma < 6.5°$ or $>173.5°$ will be detected. With a uniform distribution $A = 0.02$ in the range 2 km $\leq \lambda_z \leq$ 10 km and 25 km $\leq \lambda_h \leq$ 1000 km, 77% of the retrieved amplitudes are above 0.9 times the original ones and the observed variance will be 0.83 times the original one. Note the improvements with respect to the less realistic 2D case due to the "magnifying" effect of θ on the horizontal wavelength. In Figure 7, we plot the 3D attenuation factor $E = \exp(-\frac{R_E}{2H}\tan^2(\gamma)\cos^2(\theta))$ in terms of γ and θ ($\theta = 0$
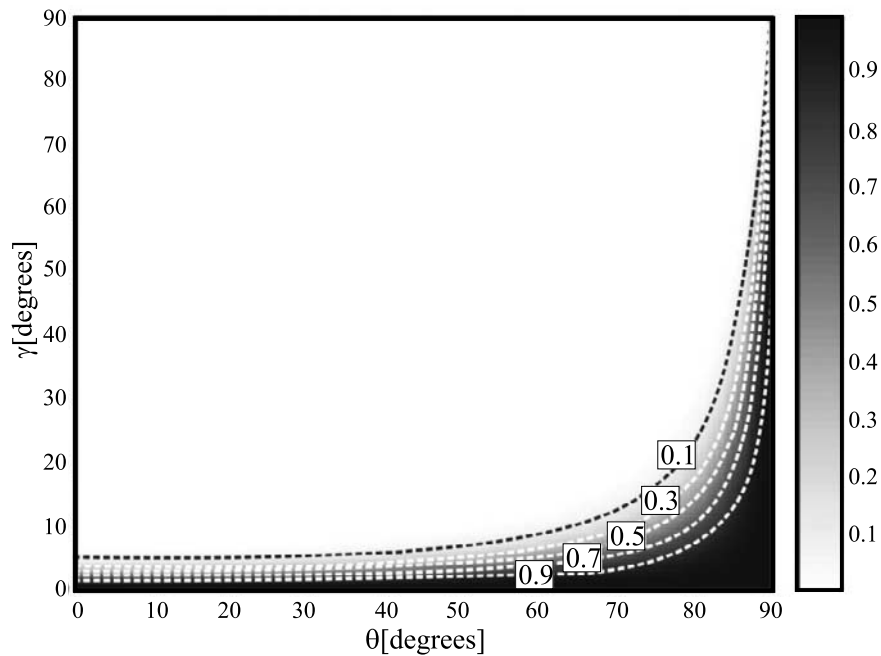

Figure 7. 3D attenuation factor between original and observed wave amplitudes E. It is represented in terms of the tilt angle of the wavefronts with respect to the horizontal surface γ and the angle θ between the LOS and the horizontal projection of the wave vector ($\gamma > \pi/4$ is probably not representative of real gravity waves).

recovers the 2D case for $\lambda_h = \lambda_x$) for the wave spectrum. It approaches 1 (no attenuation) for nearly horizontal wave phase surfaces or for the angle between LOS and horizontal wave vector tending to $\pi/2$, whereas it has a vanishing effect for wave phase surfaces approaching a vertical position. We remark that the variance reduction depends on the original wavelengths rather than on the detected ones; therefore, it is not possible in any particular occultation to account for this deficit, unless some additional information like numerical simulations is given or the preferred orientation of waves is known. The estimation of obtained against original variance seems to be robust with respect to the wave amplitude distribution. We repeated the procedures for saturated spectra usually observed in the atmosphere, with -3 and $-5/3$ slopes respectively for vertical and horizontal wavelengths [see, e.g., *Fritts and Alexander*, 2003]. A 0.02 amplitude was chosen at $\lambda_z = 10$ km and $\lambda_x = 1000$ km. In the 2D and 3D cases we respectively obtained 0.72 and 0.81 for the variance ratio, so small variations were found. This happens because the condition $R'' > 0.002$ also implies for this distribution that only the smallest horizontal wavelengths will not be detected. The unseen range is a little bit larger than in the uniform distribution and there is therefore a tiny reduction in the ratio of observed and original variance. We may conclude that the uniform distribution assumption introduces an uncertainty in variance calculation smaller than other simplifications considered in this work. In order to explicitly find out the detectable range for the saturated spectrum, A must be replaced in equation (13) by the corresponding amplitude distribution, and Figure 6 must be replaced by another representation.

[13] By calculating excess path delay of the GPS signal, *Lange and Jacobi* [2003] computed what they called visibility, the amplitude ratio between the retrieved and the original amplitudes. Their results are given by numerical solutions, whereas we obtain an analytical formulation. The present approach took into account the accuracy of the retrieval in order to find out which waves can be detected, which leads to a more restricted observable field. Notwithstanding these differences, the results on the amplitude ratio against wave numbers and the retrieved variances are similar.

[14] The smallest resolvable vertical scale is limited by the vertical sampling and retrieval processes. Any inversion method based on geometric optics limits the vertical resolution of RO retrievals to the Fresnel diffraction scales, which have been estimated at between 0.5 and 1.4 km [*Kursinski et al.*, 1997]. This may have a small impact on the results of this study because it deals with vertical wavelengths larger than 2 km. Even though wavelengths down to 0.8 km have been extracted from data [*Liou et al.*, 2006], it has been stated that noise precludes wavelengths below 2 km to be inferred [*Marquardt and Healy*, 2005]. This will render our results less accurate for the smallest vertical wavelengths. There are similar order of magnitude uncertainties due to the retrieval in the horizontal direction perpendicular to the ray, but this should be of much less concern as the resolution must in this case be compared with the horizontal wavelengths, which are typically larger than a few tenths of kilometers. In the above paragraphs, in order to obtain the results in accordance with the vertical resolution, we should, in the worst case, average uniformly over a band of parallel rays covering 1.4 km (±0.7 km around the tangent point). The value of ν_B must not be changed because the average in this region, according to the exponential law, remains nearly the same if the band is about an order of magnitude smaller than H, but we should change our calculation in one aspect: we must take an average over the interval $\phi \pm \Delta\phi$ for each m, where $\Delta\phi = m\,0.7$ km. Note that $\Delta\phi$ is smallest when m also is (the smearing effect vanishes for the largest wavelengths). However, this affects only the phase of the sinusoidal term in equation (7), which is not very significant for the determination of the response, that is mainly governed by the exponential term. Taking all these arguments into account, we just place a lower cutoff for the vertical wavelength at 2 km. We must keep in mind that all these are qualitative order of magnitude estimations.

2.2. Wavelength Distortion

[15] In the previous section, we focused on the waves amplitude response in a GPS RO retrieval, we will now concentrate on the wavelengths that the detected signal may contain and their relationship with the parameters of the original waves. It may be possible to extract information on wavelength from the measurements along the line of tangent points (LTP). The criteria of the previous section on amplitude threshold must be met, or obviously no wavelengths may be detected. The exponential weighting around every tangent point dominates for about 500 km in the horizontal direction ($2.35\sqrt{HR_E}$, see equation (4)). Note that optimum detection of wavelengths would be achieved if: (1) the LOS is nearly parallel to the wavefronts ($\theta \approx 90°$), as this would lead to a constructive rather than destructive averaging, and (2) the LTP length and direction ensure the crossing of at least two maxima or minima. IGW might in general be more accurately detected because they have a low constant phase surface tilt with respect to the horizontal plane, which is nearly parallel to the ray at the tangent point (in addition, their typical vertical wavelength is larger than the smearing height). On the contrary, short period GW have a large inclination angle and their detection may undergo a significant blurring effect as the ray crosses successive wavefronts around the tangent point (unless $\theta \approx 90°$). In any case, even if ideal conditions are met, an adequate interpretation of the results must be performed.

[16] We now approximate the LTP by a straight line, which is for many occultations a quite adequate representation. In Figure 8 we consider two successive wavefronts separated by a vertical wavelength λ_z. The h direction is defined by the horizontal projection of the wave vector and y completes a right-handed system. Note that $\lambda_y = \infty$. We may also see the LTP in the figure, where ϕ and ψ define the tilt of this straight line in the horizontal and vertical planes ($0 \leq \phi, \psi \leq \pi$). We now give an analytical derivation of the relations between the extracted and original wavelengths, but we mention that a similar deduction may be developed by geometrical means. The equations of the two successive wavefronts are

$$z_1 = \tan\gamma\ h \tag{14}$$
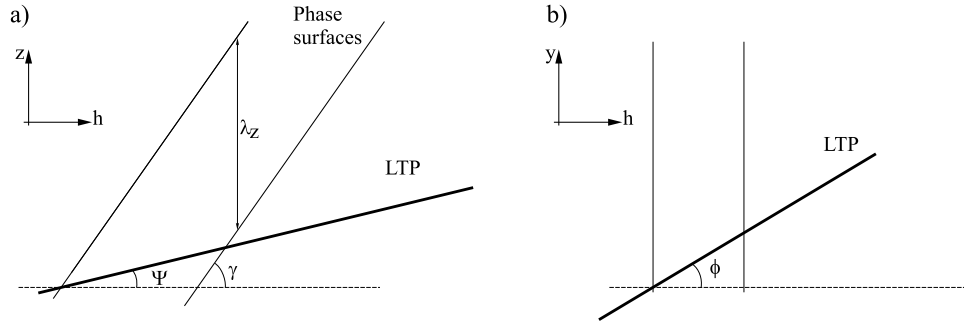
$$z_2 = \tan\gamma\ h + \lambda_z \tag{15}$$

Figure 8. A (a) vertical and (b) horizontal perspective of two successive wavefronts and the LTP of an occultation traversing them.

where $\lambda_z > 0$ and the equations defining the LTP are

$$y = \tan\phi \; h \qquad (16)$$

$$z = \tan\psi \; h \qquad (17)$$

Recall that $|\tan\gamma| = \lambda_z/\lambda_h$. If we place the origin where the LTP crosses one of the wavefronts, then some algebra shows that the next intercept will be found in

$$h_i = \frac{\lambda_z}{\tan\psi - \tan\gamma} \qquad (18)$$

$$y_i = \frac{\tan\phi \; \lambda_z}{\tan\psi - \tan\gamma} \qquad (19)$$

$$z_i = \frac{\tan\psi \; \lambda_z}{\tan\psi - \tan\gamma} \qquad (20)$$

The apparent (along LTP) horizontal and vertical wavelengths may now be calculated

$$\lambda_{h_A} = \sqrt{h_i^2 + y_i^2} = \lambda_h \frac{|\tan\gamma|}{|\tan\psi - \tan\gamma|} \frac{1}{|\cos\phi|} \qquad (21)$$

$$\lambda_{z_A} = |z_i| = \lambda_z \frac{|\tan\psi|}{|\tan\psi - \tan\gamma|} \qquad (22)$$

[17] Original wavelengths may be smaller or larger than the apparent values detected along the LTP. An estimation of the former may be done in regions where there is a generally preferred orientation of the wavefronts. The absolute values point to the fact that no information on wave motion is recovered from the available data. It should be taken into account that the horizontal coverage of occultations usually does not exceed 200 km (the horizontal resolution is of the same order, but this weakness becomes attenuated when $\theta \approx 90°$, see above), so this places an upper bound for λ_{h_A}. Even though the occultations in the neutral atmosphere cover a vertical range of about 30 km, the difficulties in appropriately modeling the tropopause may place an upper constraint of around 10 km for λ_{z_A} [see, e.g.,

Wu et al., 2006]. Some interesting limits from equations (21) and (22) of apparent wavelengths against the angles have been outlined in Table 1, where a few of them are merely academic or serve to confirm that the expected results are obtained in obvious cases. We must keep in mind that in real cases γ should be contained between nearly 0 (IGW) and $\pi/4$ (short intrinsic period GW) or equivalently between $3/4\pi$ and π, whereas ψ is usually small (between 5° and 30°, but values up to 70° may be found). In Figure 9, we plot the ratios λ_{h_A}/λ_h and λ_{z_A}/λ_z against γ and ϕ for $\psi = 10°$. Note that for λ_{h_A} when $\gamma \to 0$ and for λ_{z_A} when $\gamma \to \pi/2$ we have at first glance a $0.\infty$ condition, which is solved by replacing $|\tan(\gamma)|$ by λ_z/λ_h. We should also remark that λ_{h_A} when $\gamma \to \pi/2$ resembles the relation for LOS. This coincidence occurs because for vertical wavefronts the relation is always the same, regardless of $\psi (=0$ would mimic the LOS case). It should be stressed that the cases $\psi \to \gamma$ and $\phi \to \pi/2$, where the apparent horizontal or vertical wavelengths approach ∞, are quite unfavorable (note that if either of both apparent wavelengths exceeds the horizontal or vertical coverage of the occultation, then the apparent wavelength cannot be determined). A real horizontal wavelength may be larger than the occultation horizontal coverage and the wave will therefore stay undersampled; nevertheless, it will leave anyway its footprints on the

Table 1. Limiting Cases of Apparent Wavelengths

	λ_{h_A}		λ_{z_A}
$\gamma \to 0$	$\frac{\lambda_z}{\|\tan\psi\|}\frac{1}{\|\cos\phi\|}$		λ_z
$\gamma \to \pi/2$	$\frac{\lambda_h}{\|\cos\phi\|}$		$\lambda_h\|\tan\psi\|$
$\psi \to 0$	$\lambda_h\frac{1}{\|\cos\phi\|}$		0
$\psi \to \pi/2$	0		λ_z
$\psi \to \gamma$	∞		∞
$\tan\psi \to \tan\gamma/2$	$\lambda_h\frac{2}{\|\cos\phi\|}$		λ_z
$\tan\gamma \to \tan\psi/2$	$\lambda_h\frac{1}{\|\cos\phi\|}$		$2\lambda_z$
$\phi \to 0$	$\lambda_h\frac{\|\tan\gamma\|}{\|\tan\psi-\tan\gamma\|}$		$\lambda_z\frac{\|\tan\psi\|}{\|\tan\psi-\tan\gamma\|}$
$\phi \to \pi/2$[a]	$\frac{\|\lambda_z\|}{\|\tan\psi-\tan\gamma\|}\frac{1}{\|\cos\phi\|}$		$\lambda_z\frac{\|\tan\psi\|}{\|\tan\psi-\tan\gamma\|}$

[a]The results for $\phi = \pi/2$ are obtained when setting $\gamma = 0$ and by interpreting $\tan\psi \cos\phi = \tan\beta$, where the LTP is given by $h = 0$, $z = \tan\beta \, y$.
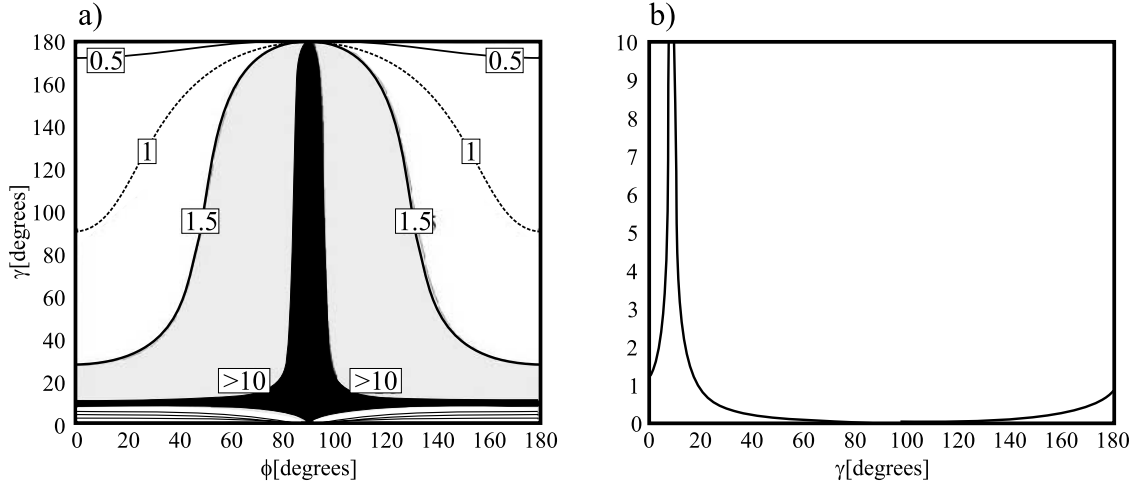
Figure 9. The ratios for tilt angle of the LTP with respect to the horizontal surface $\psi = 10°$ of apparent and original (a) horizontal wavelengths against γ (the inclination angle of the wavefronts with respect to the horizontal surface) and ϕ (the tilt angle of the LTP projection on the horizontal surface with respect to the h direction) and (b) vertical wavelengths against γ.

retrieval and will therefore contribute to the calculation of temperature variance.

[18] In brief, the observed wavelengths will always differ from the original ones, but only the presence of IGW, with $\gamma \approx 0$, will ensure small discrepancies in the vertical component.

2.3. Phase Shift

[19] We will now turn to an analysis of the phase of the original waves from the measurements along the LTP. The phase of the retrieved refractivity is governed by the term $S = \sin(\phi - \frac{k^2 R_E}{2m} + \pi/4)$. However, for each tangent point we must readapt ϕ, as equation (4) assumes that the integral is performed around $x = z = 0$, so the phase for any tangent point at $x = x_1, z = z_1$ will be $\tilde{\phi} = \phi + kx_1 + mz_1$. We must also change ν_B to $\widetilde{\nu_B} = \nu_B \exp(-z/H)$, as it is the reference value at the height of the tangent point, so

equation (4) yields for any position along the LTP

$$\hat{\nu}_1(\varrho) = \widetilde{\nu_B} A \exp\left(-\frac{1}{2}\frac{k^2}{m^2}\frac{R_E}{H}\right)\sqrt{\frac{2\pi R_E}{m}}\sin\left(\tilde{\phi} - \frac{k^2 R_E}{2m} + \pi/4\right)$$

(23)

This will not alter our previous considerations on the detection of the wavelengths, as the original phase will change by a constant factor $(-\frac{k^2 R_E}{2m} + \pi/4)$. This is the same difference between detected and original phase as found by *Preusse et al.* [2002] for an infrared limb sounder if we apply the above condition $Hm \gg 1$. As this typical atmospheric situation was not included in that work, their phase shift remained moderately dependent on altitude. In the less favorable case for $Hm \gg 1$ ($\lambda_z = 10$ km) the term associated to $\pi/4$ in their work deviates 14% from that value. The phase difference does not depend on the
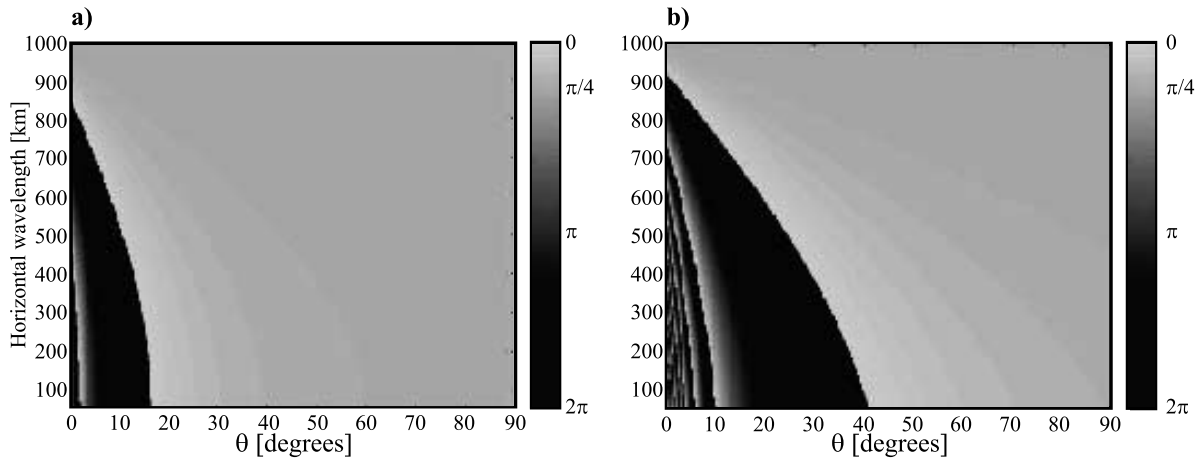

Figure 10. Phase difference modulus 2π represented in the range $0-2\pi$ between a retrieved and original wave at a fixed position. It is plotted against the original horizontal wavelength in the h direction λ_h and the angle θ between the LOS and the horizontal projection of the wave vector respectively for (a) original vertical wavelength $\lambda_z = 2$ km and (b) $\lambda_z = 10$ km.
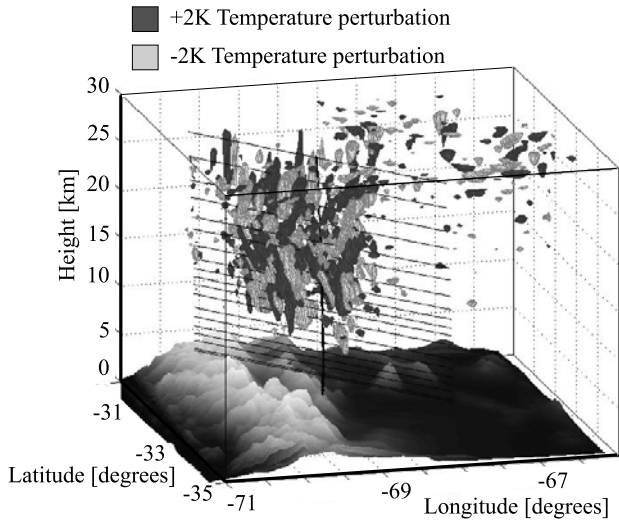
Figure 11. Wave structures as outlined by temperature perturbations of ±2 K in a numerical simulation performed for the region and time of an occultation. A 400 km long LOS is shown in each point of the LTP and topography has been included for reference. The different scales in the three axes ($1° \approx 100$ km) affect the outlook of the inclinations of the wave structures and the LTP.

position in the present work, so the wavelengths are not affected. In coincidence with this characteristic, *Belloul and Hauchecorne* [1997] found that the retrieved vertical wavelengths remain preserved with respect to the original ones (excluding the geometrical aspects of the previous section). We calculate the phase difference between exact and GPS RO retrieval for a typical case with $\lambda_h = 400$ km, $\lambda_z = 5$ km and obtain 0.16 rad. In Figure 10 we show the phase difference modulus 2π at a fixed position against λ_h and θ respectively for $\lambda_z = 2$ and 10 km. The phase shifts are clearly seen. They are characteristic for each type of detected wave (they depend on k and m). For IGW or waves approaching local spherical symmetry ($k = 0$) the shift tends to $\pi/4$.

3. Test Case

[20] In *de la Torre and Alexander* [2005] and *de la Torre et al.* [2006a] it was shown that the midlatitude region roughly between $70-65°W$ and $30-40°S$, at the eastern side of the highest Andes mountains, exhibits a significant wave activity according to occultation data, particularly in the higher troposphere and lower stratosphere. This may be caused by large amplitude MW due to the forcing of intense prevailing zonal winds blowing from the Pacific Ocean over the Andes range in the lower troposphere.

[21] We will analyze a GPS RO event that exhibited one of the strongest wave activities in this region, observed on 30 August 2001 04:09 UTC by the satellite SAC-C. The measured characteristics will be compared with a numerical simulation performed with mesoscale model WRF. This kind of models can simulate realistic GW in the troposphere and lower stratosphere, revealing 3D information that cannot be obtained by satellite measurements or which is not

available by any observational means [see, e.g., *Wu and Zhang*, 2004]. Our run was driven by initial values and assimilated lateral boundary conditions and sea surface temperatures from NCEP reanalyses. The numerical experiment employed three domains with effective horizontal grid spacing respectively of 36.0 km, 12.0 km and 4.0 km, and the top level was set at 15 mb. The simulation was initialized at 00:00 UTC on 29 August 2001.

[22] A 3D perspective of the wave structures from the numerical simulation, including the LTP, LOS and topography may be observed in Figure 11. Because of the difficulties in appropriately separating waves and background around the tropopause [see, e.g., *de la Torre et al.*, 2006b], we will consider below only the vertical range above 18 km in the occultation and simulation. The temperature variance was calculated as follows in the occultation. The temperature profile between 18 and 28 km was splined and then low-pass filtered, with a cutoff at 9 km, obtaining the background temperature. The filter applied is nonrecursive and to avoid Gibbs effects a Kaiser window was used [see, e.g., *Hamming*, 1998]. The filter was applied again to the difference between the original profile and the background temperature, now with a cutoff at 3 km, giving a result which isolates wavelengths between 3 and 9 km. Typical MW observed in the region belong to this range. The variance was calculated as $1/(10$ km) times the integral of the squared perturbation temperature integrated between 18 and 28 km of height. A similar processing was performed for the data from the numerical simulation. The region for variance calculation was restricted to 250 km around each tangent point (where the occultation weighting is strongest, see above). The ratio of observed and simulated variances was 0.65 as compared to 0.81 (for a saturated wave spectrum) expected between retrieved and original variance if all the above assumptions applied and if one was able to cleanly separate the waves of interest with respect to the background and other phenomena. In addition, above the height of about 25 km sub-Kelvin accuracy cannot be ensured. In order to perform a simple estimation of this effect, we disregard now the smearing effect of occultations. We evaluate the discrepancy introduced by the retrieval error function 0 K below 25 km altitude and +1 K above in the observed variance of a single wave with an amplitude of 4 K. A 17% difference is obtained. Finally, it must be also considered that the variance reduction estimates of the previous section assume that waves occupy all the space, for the sake of simplicity, whereas real waves look more like local packets.

4. Conclusions

[23] It is not possible to fully resolve GW from radio occultation measurements because there are different kinds of distortions. In each occultation, the outcome depends on the characteristics of the waves (essentially the wavelengths and amplitude), and on the LOS and the LTP, both with respect to the phase fronts to be detected. As already shown by *Belloul and Hauchecorne* [1997], small detected horizontal wavelength GW do not have a significant effect on the GPS RO retrieval spherical symmetry assumption, as their contribution tends to vanish by averaging through the

oscillations, but the wave might then have a faint presence in the output data. They also stated that horizontal wavelengths much larger than the horizontal distance where significant ray bending occurs (a few 100 km) have no relevant impact on the retrieval accuracy (because spherical symmetry does not break down). Finally, it was concluded that the intermediate GW range may place important doubts on the retrieval. However, we state that, rather than affecting accuracy, the observed values must be readily interpreted as the sum of a background and a perturbation value. Anyway, to elucidate the original amplitudes, wavelengths and phases in terms of the detected ones in individual soundings, some additional information, as an independent source or a region with a preferred orientation of waves is necessary.

[24] Ideal conditions for a faithful wave amplitude extraction in occultation retrievals are given by quasi horizontal wave phase surfaces or when the LOS and LTP are respectively nearly contained and out of those planes. Short horizontal scale waves are weakened or even filtered out with high probability (but not certainly, due to the "magnifying" effect on the observed horizontal wavelength when the angle between the line of sight and the horizontal wave vector approaches $\pm\pi/2$). If the temperature fluctuations represent a typical 2% of the background value, then the full observable range includes waves with phase surfaces angles in average not exceeding $6.5°$ or larger than $173.5°$ from the horizontal plane (if θ is random). For a uniform distribution of the wave spectrum in the range 2 km $\leq \lambda_z \leq$ 10 km and 25 km $\leq \lambda_x \leq$ 1000 km, 77% of the retrieved amplitudes are above 0.9 times the original ones and the observed variance will be 0.83 times the original one. Considering a more realistic amplitude distribution slightly changes the variance estimate to 0.81. The numerical simulation of the atmospheric conditions during one occultation was used to calculate the original temperature variance, and the ratio with the variance computed from the occultation data exhibited a 20% deviation from the one expected if no other phenomena than GW in the wavelength range stated in this paragraph were present. This discrepancy may be attributed to the deviation from the simplifying assumptions in obtaining that estimation and to the degree of difficulty in cleanly isolating the waves of interest in the data. Also, the decrease in temperature accuracy of GPS RO above about 25 km and the fact that real waves are local packets rather than structures occupying all space, as usually assumed, affect the variance estimates.

[25] Another result from this study is that the detected vertical wavelengths will always differ from the original ones, but only the presence of IGW, which have nearly horizontal constant phase surfaces, will ensure small discrepancies. Also, a phase difference between original and detected waves which approaches $\pi/4$ for the largest horizontal wavelengths seems to be always present. We conclude that extreme caution is needed when addressing the issues of amplitude, wavelength and phase of gravity waves in occultation data.

References

Ahmad, B., and G. L. Tyler (1998), The two-dimensional resolution kernel associated with retrieval of ionospheric and atmospheric refractivity profiles by Abelian inversion of radio occultation phase data, *Radio Sci.*, *33*, 129–142.

Alexander, M. J. (1998), Interpretations of observed climatological patterns in stratospheric gravitywave variance, *J. Geophys. Res.*, *103*, 8627–8640.

Belloul, M. B., and A. Hauchecorne (1997), Effect of periodic horizontal gradients on the retrieval of atmospheric profiles from occultation measurements, *Radio Sci.*, *32*, 469–478.

de la Torre, A., and P. Alexander (1995), The interpretation of wavelengths and periods as measured from atmospheric balloons, *J. Appl. Meteorol.*, *34*, 2747–2754.

de la Torre, A., and P. Alexander (2005), Gravity waves above Andes detected from GPS radio occultation temperature profiles: Mountain forcing?, *Geophys. Res. Lett.*, *32*, L17815, doi:10.1029/2005GL022959.

de la Torre, A., P. Alexander, C. Menéndez, T. Schmidt, and J. Wickert (2006a), Gravity waves above the Andes detected from GPS radio occultation temperature profiles: Jet mechanism?, *Geophys. Res. Lett.*, *33*, L24810, doi:10.1029/2006GL027343.

de la Torre, A., T. Schmidt, and J. Wickert (2006b), A global analysis of wave potential energy in the lower stratosphere derived from 5 years of GPS radio occultation data with CHAMP, *Geophys. Res. Lett.*, *33*, L24809, doi:10.1029/2006GL027696.

Eckermann, S. D., D. E. Gibson-Wilde, and J. T. Bacmeister (1998), Gravity wave perturbations of minor constituents: A parcel advection methodology, *J. Atmos. Sci.*, *55*, 3521–3539.

Fjeldbo, G., A. J. Kliore, and V. R. Eshleman (1971), The neutral atmosphere of Venus as studied with the Mariner V radio occultation experiments, *Astron. J.*, *76*, 123–140.

Fritts, D. C., and J. Alexander (2003), Gravity wave dynamics and effects in the middle atmosphere, *Rev. Geophys.*, *41*(1), 1003, doi:10.1029/2001RG000106.

Gorbunov, M. E. (1990), Solution of inverse problems of remote atmospheric refractometry on limb paths, *Izv. Russ. Acad. Sci. Atmos. Ocean. Phys., Engl. Transl.*, *26*, 86–91.

Gradshteyn, I. S. and I. M. Ryzhik (1965), *Table of Integrals, Series and Products*, Elsevier, New York.

Hamming, R. W. (1998), *Digital Filters*, 3rd ed., Dover Publications, Mineola, New York.

Kuo, Y.-H., T.-K. Wee, S. Sokolovskiy, C. Rocken, W. Schreiner, D. Hunt, and R. Anthes (2004), Inversion and error estimation of GPS radio occultation data, *J. Meteorol. Soc. Jpn.*, *82*, 507–531.

Kursinski, E. R., G. A. Hajj, K. R. Hardy, J. T. Schofield, and R. Linfield (1997), Observing Earth's atmosphere with radio occultation measurements using the Global Positioning System, *J. Geophys. Res.*, *102*, 23,429–23,465.

Lange, M., and C. Jacobi (2003), Analysis of gravity waves from radio occultation measurements, in *First CHAMP Mission Results for Gravity, Magnetic and Atmospheric Studies*, edited by C. Reighber, H. Lühr, and P. Schwintzer, pp. 479–484, Springer, New York.

Liou, Y. A., A. G. Pavelyev, J. Wickert, S. F. Liu, A. A. Pavelyev, T. Schmidt, and K. Igarashi (2006), Application of GPS radio occultation method for observation of the internal waves in the atmosphere, *J. Geophys. Res.*, *111*, D06104, doi:10.1029/2005JD005823.

Lusignan, B., G. Modrell, A. Morrison, J. Pomalaza, and S. G. Ungar (1969), Sensing the Earth's atmosphere with occultation satellites, *Proc. IEEE*, *4*, 458–467.

Marquardt, C., and S. B. Healy (2005), Measurement noise and stratospheric gravity wave characteristics obtained from GPS occultation data, *J. Meteorol. Soc. Jpn.*, *83*, 417–428.

Preusse, P., et al. (2002), Space-based measurements of stratospheric mountain waves by CRISTA: 1. Sensitivity, analysis method, and a case study, *J. Geophys. Res.*, *107*(D23), 8178, doi:10.1029/2001JD000699.

Ratnam, M. V., M. Tetzlaff, and C. Jacobi (2004), Global and seasonal variations of stratospheric gravity wave activity deduced from the CHAMP/GPS satellite, *J. Atmos. Sci.*, *61*, 1610–1620.

Rieder, M. J., and G. Kirchengast (2001), Error analysis and characterization of atmospheric profiles retrieved from GNSS occultation data, *J. Geophys. Res.*, *106*, 31,755–31,770.

Schreiner, W., C. Rocken, S. Sokolovskiy, S. Syndergaard, and D. Hunt (2007), Estimates of the precision of GPS radio occultations from the COSMIC/FORMOSAT-3 mission, *Geophys. Res. Lett.*, *34*, L04808, doi:10.1029/2006GL027557.

Tsuda, T., M. Nishida, C. Rocken, and R. H. Ware (2000), A global morphology of gravity wave activity in the stratosphere revealed by the GPS occultation data (GPS/MET), *J. Geophys. Res.*, *105*, 7257–7273.

Wu, D. L., and J. W. Waters (1996), Satellite observations of atmospheric variances: A possible indication of gravity waves, *Geophys. Res. Lett.*, *23*, 3631–3634.

Wu, D. L., and F. Zhang (2004), A study of mesoscale gravity waves over the North Atlantic with satellite observations and a mesoscale model, *J. Geophys. Res.*, *109*, D22104, doi:10.1029/2004JD005090.

Wu, D. L., et al. (2006), Remote sounding of atmospheric gravity waves with satellite limb and nadir techniques, *Adv. Space Res.*, *37*, 2269–2277.

Yunck, T. P. (2002), An overview of atmospheric radio occultation, *J. Global Positioning Syst.*, *1*, 58–60.

_____

P. Alexander, A. de la Torre, and P. Llamedo, Departamento de Física, Facultad de Ciencias Exactas y Naturales, Universidad de Buenos Aires, Ciudad Universitaria, 1428 Buenos Aires, Argentina. (peter@df.uba.ar)